# CFD SIMULATION OF CRITICAL HEAT FLUX IN A TUBE

**L. Vyskocil, J. Macek**

*Nuclear Research Institute Rez (NRI), Dept. of Thermal Hydraulic Analyses,*
*250 68 Rez, Czech Republic*

**Abstract**

This paper presents numerical simulations of the boiling flow in a tube with a Departure from Nucleate Boiling type of critical heat flux (CHF). Standard tables of CHF produced by the Russian Academy of Sciences were used as a data set. The simulations were performed with the multiphase code NEPTUNE_CFD V1.0.7. A simple criterion based on the void fraction at the wall was used for the CHF prediction. Four data series were selected from the tables. In every series, one of the following parameters was variable: the local equilibrium quality, the mass flux, pressure and the tube diameter. The remaining three parameters were fixed. In every data point, a numerical simulation was performed so as to find out the interval of the wall heat fluxes at which the boiling crisis occurs.

NEPTUNE was able to quite accurately predict CHF in cases with high mass fluxes and high pressures. On the other hand, in one low-mass-flux case, the CHF in the calculation occurred at a wall heat flux as low as 80% of the experimental heat flux. In low pressure cases, a stable solution could not be obtained due to numerical oscillations.

The presented work was carried out within the 7th FP EURATOM NURISP project. NEPTUNE_CFD code is implemented in the NURESIM platform.

## 1. INTRODUCTION

Flow nucleate boiling has a high heat transfer coefficient. This efficient heat transfer mechanism, however, is limited by a critical heat flux (CHF). Above the critical heat flux, benign nucleate boiling is transformed to a film boiling with poor heat transfer. In a heat-flux-controlled system, this transition of the boiling mechanism is characterized by a sudden rise in the surface temperature due to the drop in the heat transfer coefficient. Determining the critical heat flux is one of the important issues in nuclear reactor safety.

The prediction of two-phase flow parameters distribution, especially the void fraction, is an attractive and challenging subject. Among various two-phase flow models, the three-dimensional two-fluid model by Ishii (1990) is an effective tool for predicting parameters distribution in two-phase systems. Many papers dealing with the CFD simulation of a boiling bubbly flow using the two-fluid model can be found in open literature. To name a few, we mention here the work of Yao and Morel (2002, 2004), Koncar and Borut (2008) and Troshko et al. (2007).

On the other hand, there are only a few reports on CFD simulation of a boiling flow under CHF conditions. Morel (2006) and Vyskocil and Macek (2008) demonstrated that CFD codes can be used to simulate a boiling flow close to the DNB (departure from nucleate boiling) condition in the DEBORA experiment. Shin and Chang (2008) successfully simulated a boiling flow under the CHF condition in a rod bundle with and without a mixing vane.

Some attempts have been made to create a criterion for predicting CHF in CFD from the local flow parameters. The report of Haynes et al. (2006) presents a "Local Predictive Approach" anticipating a better prediction of DNB in CFD. Weisman and Pei (1983) developed a mechanistic model for predicting CHF in a channel. In their model, a local void fraction equal to 0.82 was used as a criterion for predicting CHF. Podowski and Podowski (2009) proposed a more complicated CHF criterion. Two conditions must be satisfied simultaneously to avoid CHF: the void fraction cannot exceed 0.74 and the distance between the previously formed bubble and the heated wall must be at least equal to the bubble diameter when the new bubble starts to form. Le Corre et al. (2010) presented DNB criterion based on local overheating underneath a nucleating bubble.

The goal of the work presented in this report was to assess the capability of NEPTUNE_CFD code to simulate a boiling flow with the DNB type of critical heat flux in tube geometry. NEPTUNE_CFD

is a multiphase CFD code developed jointly by EDF R&D and CEA. A simple criterion based on a local void fraction was used to predict CHF in our work.

## 2. MODELING BOILING FLOW UNDER CHF CONDITIONS

This chapter describes the generalized boiling model, which is implemented in NEPTUNE code and used for numerical simulations of CHF. The presented model simulates the onset of nucleate boiling, partitioning of the wall heat flux and interfacial liquid-vapour heat, momentum and mass transfer.

Two phases are modelled: the primary phase is liquid and the secondary is vapour bubbles. The same pressure is shared by the two phases. Continuity, momentum and energy equations are solved for each phase. The "k-ε liq" model (Yao, Morel 2004) is used for modelling the liquid turbulence; the flow of vapour is assumed to be laminar. The distribution of the mean bubble diameter in the flow is modelled using a one-group interfacial area transport equation.

### 2.1 Onset of Nucleate Boiling

When the wall becomes superheated, vapour bubbles can form even when the core liquid is still sub-cooled. The position where the first bubbles occur at the wall is denoted as the onset of nucleate boiling. In our calculations, Hsu's criterion is used to determine this position (Hsu, 1962). According to this criterion, a bubble will grow from a vapour embryo occupying a cavity in the wall if the liquid temperature at the tip of the embryo is at least equal to the saturation temperature corresponding to the bubble pressure.

### 2.2 Basic Wall Heat Flux Partitioning Model

The heat flux partitioning model of Kurul and Podowski (1990) (see also Yao, Morel 2002, 2004) has the following structure:

Downstream of the onset of nucleate boiling, the wall heat flux $q_{wall}$ is split into three parts:

$$q_{wall} = q_f + q_q + q_e \quad \left[W/m^2\right] \tag{1}$$

The first part is the single-phase heat transfer (convective heat flux):

$$q_f = A_1 \alpha_{wallfcn} \left(T_{wall} - T_l\right) \tag{2}$$

$$A_1 = 1 - A_2 \tag{3}$$

$A_1$ is the fraction of the wall surface influenced by the liquid, fraction $A_2$ is influenced by vapour bubbles formed on the wall, $T_l$ is the liquid temperature at the centre of the wall adjacent cell, $\alpha_{wallfcn}$ is the wall heat transfer coefficient calculated from the temperature wall function.

The quenching part $q_q$ of the heat flux $q_{wall}$ is transported by transient conduction during the time period between the bubble departure and the next bubble formation at the same nucleation site.

$$q_q = A_2 \alpha_{quench} \left(T_{wall} - T_l\right) \tag{4}$$

$\alpha_{quench}$ is the quenching heat transfer coefficient (11).

Heat flux $q_e$ is spent for liquid evaporation:

$$q_e = \dot{m}_e H_{lat} \tag{5}$$

$\dot{m}_e$ is the evaporation mass transfer per the unit wall area (9), $H_{lat}$ is the latent heat.

The model assumes that the diameter of the area influenced by a single bubble is as large as the bubble departure diameter $d_w$:

$$A_2 = \min\left(\frac{\pi \cdot d_w^{\,2} \cdot n}{4}, 1\right) \tag{6}$$

n is the active nucleation site density. The bubble departure diameter $d_w$ is calculated from Ünal correlation (Ünal, 1976). The active nucleation site density is correlated to the wall superheat:

$$n = \left(210 \cdot \left(T_{wall} - T_{sat}\right)\right)^{1.8} \quad \left[m^{-2}\right] \tag{7}$$

To calculate the evaporation rate $\dot{m}_e$, the bubble detachment frequency f is determined from the following equation:

$$f = \sqrt{\frac{4 \cdot g \cdot (\rho_l - \rho_v)}{3 \cdot d_w \cdot \rho_l}} \quad \left[\frac{1}{s}\right] \tag{8}$$

The evaporation rate is the product of bubble mass, detachment frequency and the active nucleation site density:

$$\dot{m}_e = \frac{\pi \cdot d_w^{\,3}}{6} \rho_v \cdot f \cdot n \quad \left[\frac{kg}{m^2 s}\right] \tag{9}$$

The quenching heat transfer coefficient $\alpha_{quench}$ depends on the waiting time between bubble departure and the next bubble formation. This waiting time $t_w$ is fixed to the bubble detachment period:

$$t_w = \frac{1}{f} \quad [s] \tag{10}$$

$$\alpha_{quench} = 2 \cdot \lambda_l \cdot f \cdot \sqrt{\frac{t_w}{\pi \cdot a_l}} \quad \left[\frac{W}{m^2 K}\right] \tag{11}$$

where $a_l$ is the liquid thermal diffusivity.

### 2.3 Generalization of the Wall Heat Flux Partitioning Model

The basic wall heat flux partitioning model presented in chapter 2.2 assumes that the amount of water on the wall is sufficient to remove heat from the wall and to be used for evaporation. Superheating of the vapour that occurs at high void fractions is not modelled. Given all this, the basic heat flux partitioning model cannot be used under critical heat flux conditions.

In order to account for a critical heat flux condition, the heat flux partitioning model can be generalized as follows:

$$q_{wall} = f_{\alpha 1}\left(q_f + q_q + q_e\right) + \left(1 - f_{\alpha 1}\right) q_v \quad \left[W / m^2\right] \tag{12}$$

A fourth part of the wall heat flux, $q_v$, is the diffusive heat flux given to the vapour phase:

$$q_v = \alpha_{wallfcn,v}\left(T_{wall} - T_v\right) \tag{13}$$

$\alpha_{wallfcn,v}$ is the wall heat transfer coefficient calculated from the temperature wall function for the vapour phase, $T_v$ is the vapour temperature at the centre of the wall-adjacent cell. $f_{\alpha 1}$ is the phenomenological function, which depends on the liquid volume fraction $\alpha_1$. The "EDF wall-fluid heat transfer" model (see Lavieville et al. 2005) that is implemented in NEPTUNE and used in our calculations assumes function $f_{\alpha 1}$ in the following form:

$$\alpha_1 > \alpha_{1,crit}: \quad f_{\alpha 1} = 1 - \frac{1}{2}\exp\left[-20\left(\alpha_1 - \alpha_{1,crit}\right)\right] \tag{14}$$

$$\alpha_1 < \alpha_{1,crit}: \quad f_{\alpha 1} = \frac{1}{2}\left(\frac{\alpha_1}{\alpha_{1,crit}}\right)^{20\alpha_{1,crit}} \tag{15}$$

$$\alpha_{1,crit} = 0.2$$

The critical value for the void fraction is $1 - \alpha_{1,crit} = 0.8$. In our calculations, a local void fraction equal to 0.8 is used as a criterion for the CHF. Note that Weisman DNB criterion is a void fraction equal to 0.82 (Weisman and Pei 1983).

### 2.4 Interfacial Momentum Transfer

The interfacial momentum transfer was modelled by the four forces: drag force, added mass force, lift force and turbulent dispersion force (Lance, Lopez de Bertodano, 1994, Yao, Morel 2002, 2004). Wall lubrication force was not modelled. The drag coefficient $c_D$ was calculated by the Inclusions (EDF) model (Lavieville et al. 2005). The lift coefficient was $c_L = 0.29$. The added mass force coefficient was $c_{AM} = 0.5$. The turbulent dispersion coefficient $c_{TD}$ was calculated from the drag and virtual mass forces.

### 2.5 Interfacial Heat Transfer

The interface to liquid heat transfer was modelled by an "ASTRID-like model" (Lavieville et al. 2005). The interface to vapour heat transfer is calculated with help of the "constant time scale return to saturation" method (Lavieville et al. 2005). The interfacial mass transfer was calculated directly from the interfacial heat transfer.

### 2.6 Interfacial Area Transport

The Sauter mean bubble diameter distribution in the flow is calculated from the interfacial area concentration. The one-group equation of the interfacial area concentration transport with models for coalescence and break-up (Yao and Morel 2004; Morel, Yao, Bestion, 2003) is used to describe the evolution of the interfacial area concentration.

## 3. TABLES OF CRITICAL HEAT FLUX

The Russian Academy of Sciences produced a series of standard tables of critical heat flux in a tube as a function of the **local** bulk mean water condition and for various pressures and mass velocities for a fixed tube diameter of 8 mm (Collier, 1981, USSR Academy of Sciences, 1976). The tables are valid for $z/D \geq 20$. For tube diameters other than 8 mm the critical heat flux is given by the approximate relationship:

$$q_{crit} = q_{crit,8mm}\left(\frac{8}{D[mm]}\right)^{0.5} \quad \text{for } 4\text{mm} \leq D \leq 16 \text{ mm} \tag{16}$$

These tables were used as the data set for our simulations. A consistency check was performed with Groeneveld Look-Up Tables (Groeneveld, 1986). The interpolated values from the Groeneveld tables agree well with the CHF values provided by the tables of The Russian Academy of Sciences.

## 4. SIMULATION OF CHF IN NEPTUNE

### 4.1 Computational Grid

The computational domain covers 10° wedge section of a tube confined by symmetry planes and a portion of wall. The resolution of the base grid is 20x(200+400+200) cells for a 0.5 m long inlet adiabatic section, a 1m long heated section and a 0.5 m long outlet adiabatic section. For stability reasons, wedge cells in the tube centre were omitted and replaced by a small symmetry plane. Solution grid independence was tested on a fine grid (30x1200 cells) and on a coarse grid (14x560 cells), see section 5.1.

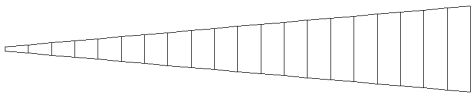

Fig. 1: Computational grid – horizontal cross section

The "k-ε liq" model (Yao, Morel 2004) with standard single-phase wall functions was used in our simulations. The thickness of the wall-adjacent cells was chosen so that each wall-adjacent cell's centroid was located within the log-law layer, $30 < y^+ < 300$. The flow parameters used in the Ünal correlation (Ünal, 1976) were calculated from the non-dimensional distance $y^+ = 250$ rather than from the centre of the wall-adjacent cell so as to assure the grid-independence of the wall-heat-flux partitioning model.

### 4.2 Calculation Procedure

The inlet temperature was calculated from the mass flux, local equilibrium quality and critical heat flux from the tables. This inlet temperature was used as a boundary condition. The heated length was

set to 1 m. In some cases, a longer or shorter heated length had to be used so as to keep the inlet temperature below boiling and above freezing point for the given local conditions.

The calculation was started with a wall heat flux equal to the CHF from the tables. When the flow rate (liquid + vapour) leaving the domain was equal to the inlet flow rate and the wall temperatures and other parameters were stabilized, the results were analyzed. Depending on the results, the wall heat flux was after this decreased or increased so as to find the interval of the wall heat flux in which the void fraction exceeds the critical value of 0.8.

## 5. DETAILED RESULTS FOR ONE DATA POINT

Four series of data were selected from the tables and simulated by NEPTUNE_CFD code. These series intersect at data point "Case 6" (p = 15.7MPa, G = 2000kg/m$^2$/s, $X_{eq}$ = 0, D = 8mm). This chapter presents the calculated results for "Case 6" in detail. The results of the other cases are similar and will be summarized in the next chapter.

Fig. 2 presents the evolution of temperatures along the tube length. The heated length begins at the vertical coordinate z = 0m and ends at z = 1m. There is a single-phase convective heat transfer to the liquid at the beginning of the heated section. The wall temperature is below that necessary for nucleation and the liquid is being heated up. At approximately z = 0.1m, the conditions adjacent to the wall are such that the formation of vapour from nucleation sites can occur. The wall temperature is above the saturation temperature but the liquid is still sub-cooled. The beginning of nucleation can be seen in Fig. 3 (see the blue line, 100% wall heat flux). At some point along the tube (z~0.7m), the liquid temperature in the centre of wall-adjacent cell reaches the saturation temperature (Fig. 2, blue line) but the liquid in the core is still sub-cooled (Fig. 5). Near the end of heated section (z~0.88m), the void fraction on the heated wall exceeds the critical value of 0.8 (Fig. 3, blue line), the wall temperature rapidly increases (Fig. 2, black line) and the vapour becomes superheated (Fig. 2, red line). The sudden increase in the wall temperature is directly connected with the void fraction, see the equations in chapter 2.3. This behaviour of the wall temperature was observed in all calculated cases.

After leaving the heated section, vapour condenses (see Fig. 3, blue line; and Fig. 4) and the liquid in the core reaches the saturation temperature (Fig. 5). Note that the exit equilibrium quality in this case is $X_{eq}$=0.

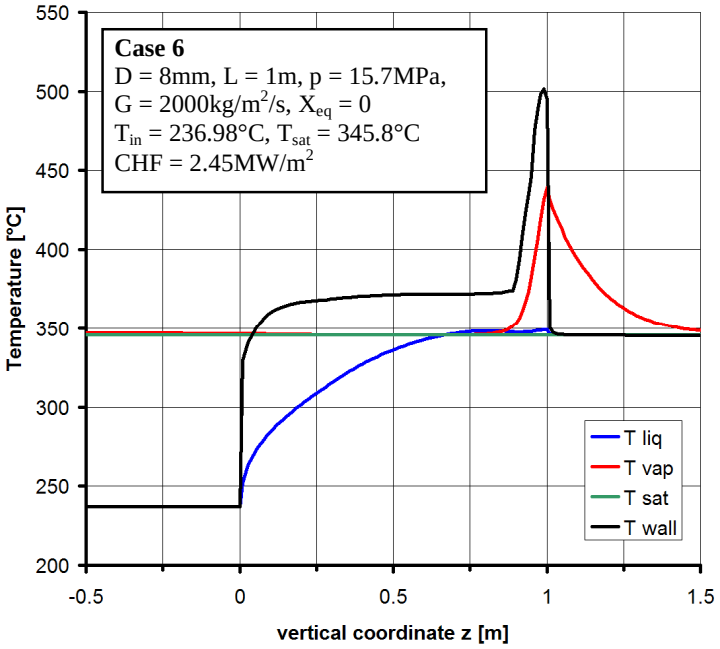


Fig. 2: Calculated temperatures along the tube length (Case 6)

**T liq** - liquid temperature in the centre of wall-adjacent cell, **T vap** - vapour temperature in the centre of the wall-adjacent cell, **T sat** - saturation temperature, **T wall** - temperature of the wall surface

Fig. 3 shows the evolution of the void fraction along the heated wall for different wall heat fluxes. 100% wall heat flux means that the critical heat flux from the CHF tables was used in the calculation, 90% means that the wall heat flux used in the calculation was 0.9·CHF and so on. The inlet conditions are fixed. It can be seen that the maximum calculated void fraction depends on the wall heat flux and can be used as a parameter for predicting CHF. In this case, the simulation was successful because a wall heat flux equal to CHF caused a sudden increase in the wall temperature at the end of the heated section (the void fraction exceeded the critical value of 0.8). When a wall heat flux equal to 0.9·CHF was used in the calculation, the calculated maximum void fraction was below the critical value.

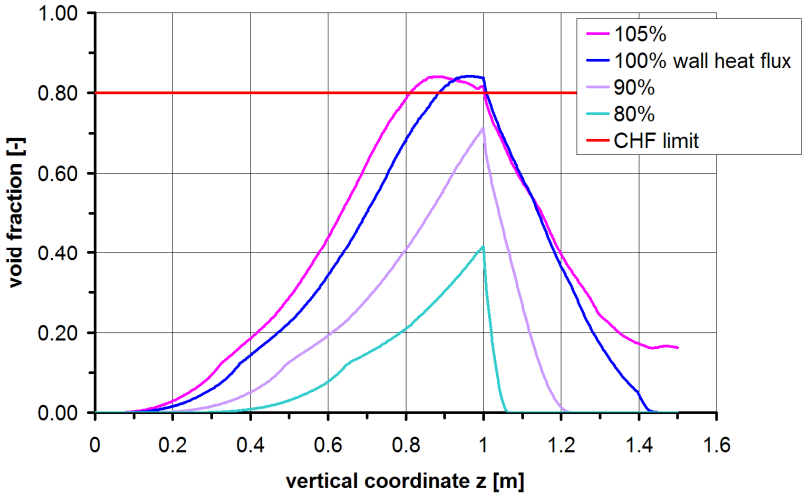


Fig. 3: Case 6: Evolution of the void fraction along the heated wall for different wall heat fluxes

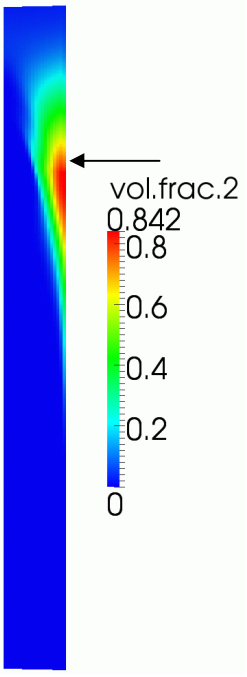


Fig. 4: Case 6: void fraction [-]
(arrow: end of heated section)

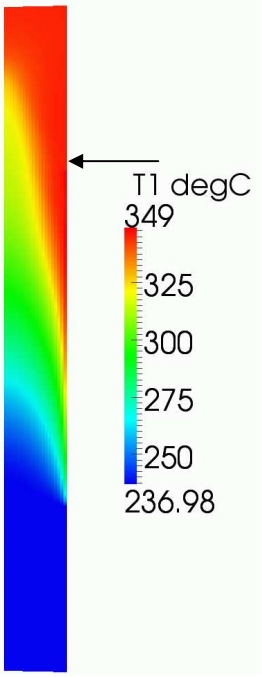


Fig. 5: Case 6: Liquid temperature [°C]
(arrow: end of heated section)

Note: the calculation domain in Fig. 4 and Fig. 5 is vertically shrunk for visualization. The actual tube diameter is 8mm, the tube length including the adiabatic inlet and outlet part is 2m. The tube axis is on the left side and the heated wall is on the right side of the computational domain.

### 5.1 Solution Grid Independence Test

The CHF criterion in our calculations is based on the void fraction near the wall. This test shows the dependence of the maximum calculated void fraction on grid resolution. Case 6 was calculated on three different grids, the results are shown in Fig. 6.

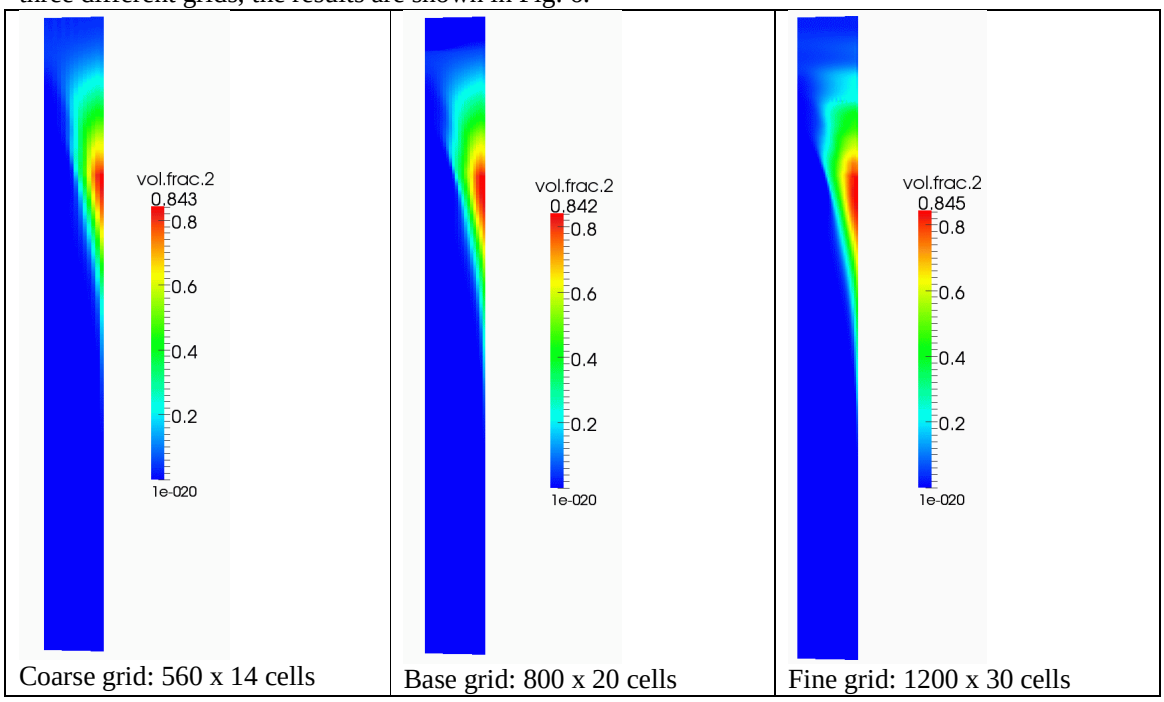


Fig. 6: Case 6: Void fraction [-], solution grid independence test

The maximum calculated void fraction is almost independent of the grid resolution. The base grid is fine enough and using finer grid gives no advantage.

## 6. SUMMARY OF THE RESULTS FOR THE SELECTED DATA SERIES

This section summarizes the results of all selected data points. Four series of data points were selected from the CHF tables. A table and chart is provided for each series. The table shows the parameters of the data points. The last column of the table shows the calculated maximum void fraction for a calculation with 100% wall heat flux (i.e. CHF from the CHF tables). The chart shows the dependence of the calculated maximum void fraction on the heat flux adjusted in the calculation for the data points in the given data series. The purpose of the chart is to show the capability of the NEPTUNE_CFD code to predict CHF.

The meaning of the symbols in the tables and charts is as follows:
D - tube diameter, p – pressure, G – mass flux, $X_{eq}$ – local equilibrium quality, CHF – critical heat flux from the tables, L - heated length, $T_{inlet}$ - inlet temperature, $T_{sat}$ - saturation temperature,
$\alpha_{max}$ - calculated maximum void fraction for calculation with 100% wall heat flux i.e. CHF.

**100% wall heat flux:** the maximum void fraction in calculations with 100% wall heat flux (= critical heat flux from the tables)
**90% wall heat flux**: calculations with the wall heat flux decreased to 90% of CHF, the inlet parameters are fixed
**CHF limit:** CHF criterion – a void fraction equal to 0.8

### 6.1 Data Series 1

The simulations of cases in this series were successful; the CHF predicted in the calculation was within the range 90-100% of the CHF from the tables (see Fig. 7).

Note: According to the two-phase flow regime map by Hewitt and Roberts (1969) and the criterion for the transition to annular flow by Taitel et al. (1980), the last two data points in Series 1 with the highest quality are the dryout type of CHF. The generalized boiling model presented in this paper assumes a bubbly flow with a DNB-type of boiling crisis.

Table 1: Series 1 (variable local equilibrium quality $X_{eq}$)

| | D | p | G | $X_{eq}$ | CHF | L | $T_{inlet}$ | $T_{sat}$ | $\alpha_{max}$ |
|---|---|---|---|---|---|---|---|---|---|
| | [m] | [MPa] | [kg/m$^2$/s] | [-] | [MW/m$^2$] | [m] | [°C] | [°C] | [-] |
| Case 4 | 0.008 | 15.7 | 2000 | 0.2 | 1.25 | 1 | 329.88 | 345.8 | 0.783 |
| Case 5 | 0.008 | 15.7 | 2000 | 0.1 | 1.75 | 1 | 292.18 | 345.8 | 0.818 |
| Case 6 | 0.008 | 15.7 | 2000 | 0 | 2.45 | 1 | 236.98 | 345.8 | 0.842 |
| Case 7 | 0.008 | 15.7 | 2000 | -0.0845 | 3 | 1 | 188.37 | 345.8 | 0.835 |
| Case 8 | 0.008 | 15.7 | 2000 | -0.1892 | 3.65 | 1 | 127.19 | 345.8 | 0.827 |
| Case 9 | 0.008 | 15.7 | 2000 | -0.339 | 4.5 | 1 | 42.05 | 345.8 | 0.82 |
| Case 10 | 0.008 | 15.7 | 2000 | -0.4737 | 5.4 | 0.8 | 21.94 | 345.8 | 0.807 |

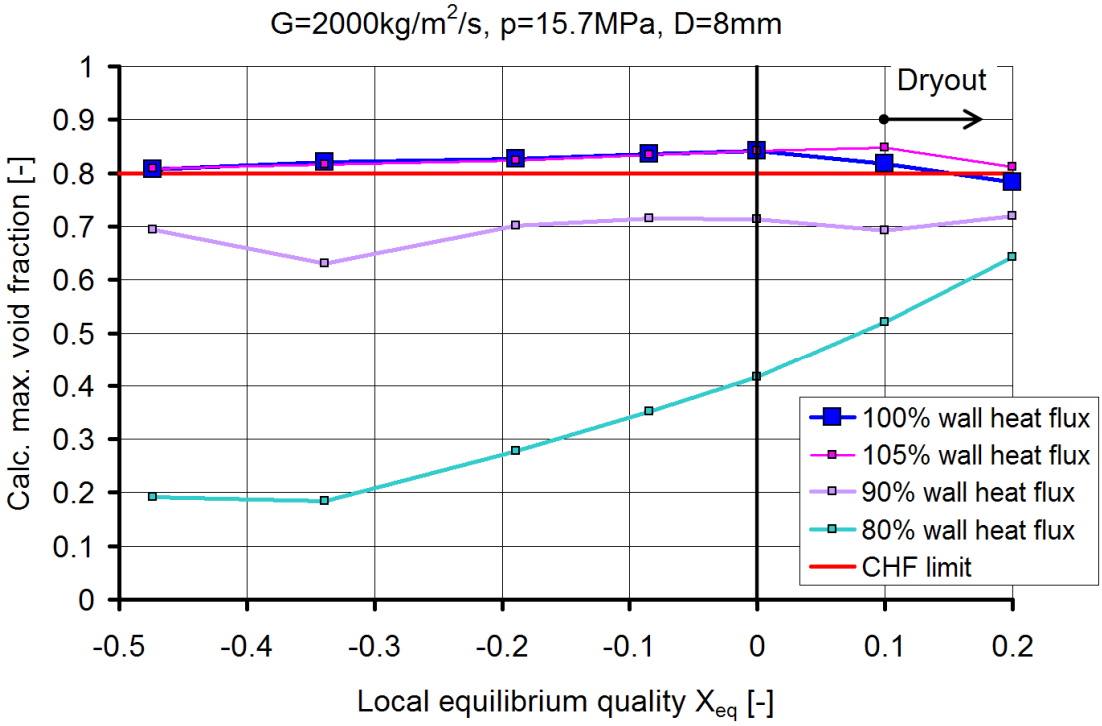


Fig. 7: Series 1 - Results

### 6.2 Data Series 2

It can be seen in Fig. 8 that the presented method of CHF prediction does not work for low mass fluxes. See data point G = 1000kg/m$^2$/s. At this data point, a wall heat flux equal to 0.7·CHF is enough for the void fraction to approach the critical value of 0.8. A similar problem with mass flux is present in the model of Weisman and Pei (1983); their model is limited to mass fluxes above 970 kg/m$^2$/s.

In the high mass flux cases (G ≥ 3000kg/m$^2$/s), 105% wall heat flux was needed for the void fraction to exceed the critical value.

Table 2: Series 2 (variable mass flux G)

| | D | p | G | $X_{eq}$ | CHF | L | $T_{inlet}$ | $T_{sat}$ | $\alpha_{max}$ |
|---|---|---|---|---|---|---|---|---|---|
| | [m] | [MPa] | [kg/m$^2$/s] | [-] | [MW/m$^2$] | [m] | [°C] | [°C] | [-] |
| Case 17 | 0.008 | 15.7 | 5000 | 0 | 3.75 | 1 | 285.9 | 345.8 | 0.798 |
| Case 16 | 0.008 | 15.7 | 4000 | 0 | 3.15 | 1 | 282.25 | 345.8 | 0.746 |
| Case 15 | 0.008 | 15.7 | 3000 | 0 | 2.85 | 1 | 265.96 | 345.8 | 0.785 |
| Case 14 | 0.008 | 15.7 | 2500 | 0 | 2.65 | 1 | 254.55 | 345.8 | 0.819 |
| Case 6 | 0.008 | 15.7 | 2000 | 0 | 2.45 | 1 | 236.98 | 345.8 | 0.842 |
| Case 11 | 0.008 | 15.7 | 1500 | 0 | 2.3 | 1 | 202.86 | 345.8 | 0.83 |
| Case 12 | 0.008 | 15.7 | 1000 | 0 | 2.1 | 1 | 137.29 | 345.8 | 0.821 |
| Case 13 | 0.008 | 15.7 | 750 | 0 | 2 | 0.8 | 133.35 | 345.8 | 0.787 |

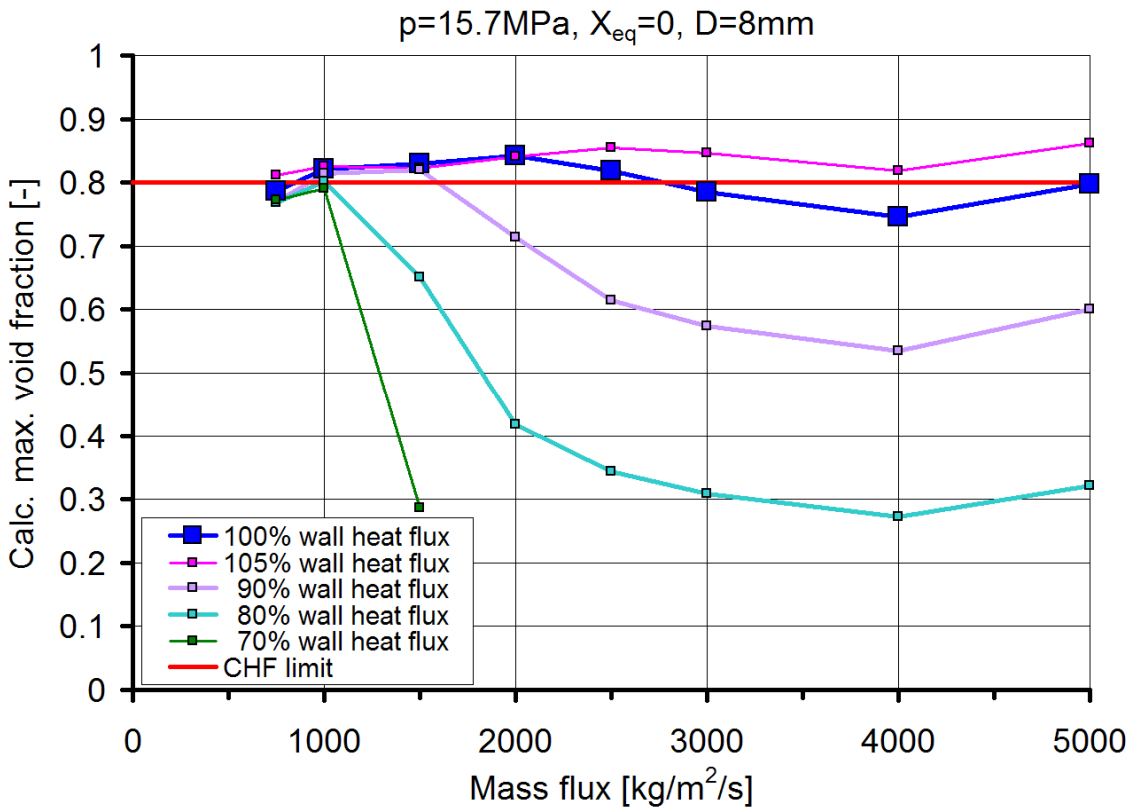


Fig. 8: Series 2 - Results

### 6.3 Data Series 3

Calculations at low pressures provided oscillating solutions that could not be stabilized. This behaviour might be related to the size of the bubbles. The bubbles are larger at low pressure and far from spherical and the models for interfacial momentum, heat and mass transfer used in this work are no longer suitable for these bubbles. The presented method of CHF prediction works well for higher pressures.

Table 3: Series 3 (variable pressure p)

| | D | p | G | $X_{eq}$ | CHF | L | $T_{inlet}$ | $T_{sat}$ | $\alpha_{max}$ |
|---|---|---|---|---|---|---|---|---|---|
| | [m] | [MPa] | [kg/m$^2$/s] | [-] | [MW/m$^2$] | [m] | [°C] | [°C] | [-] |
| Case 22 | 0.008 | 9.8 | 2000 | 0 | 4.45 | 1 | 66.56 | 309.52 | 0.85 |
| Case 20 | 0.008 | 11.8 | 2000 | 0 | 3.55 | 1 | 139.77 | 323.39 | 0.816 |
| Case 18 | 0.008 | 13.7 | 2000 | 0 | 3.1 | 1 | 183.28 | 334.96 | 0.82 |
| Case 6 | 0.008 | 15.7 | 2000 | 0 | 2.45 | 1 | 236.98 | 345.8 | 0.842 |
| Case 19 | 0.008 | 17.6 | 2000 | 0 | 2.1 | 1 | 271.56 | 355.14 | 0.829 |
| Case 21 | 0.008 | 19.6 | 2000 | 0 | 1.65 | 1 | 310.86 | 364.06 | 0.811 |

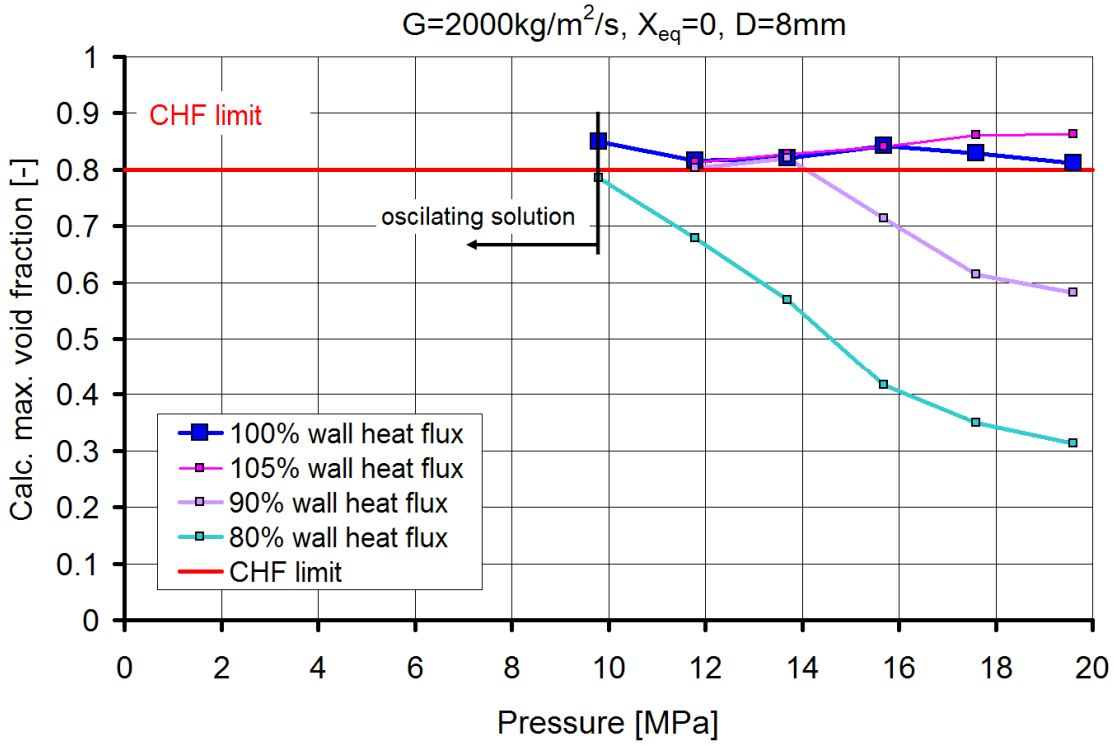


Fig. 9: Series 3 - Results

### 6.4 Data Series 4

Simulations of cases in this series were successful; the CHF predicted in the calculation was within the range of 90-100% of the CHF from the tables (see Fig. 10).

Note: the CHF figures in Series 4 were calculated from the approximate relationship (16).

Table 4: Series 4 (variable tube diameter D)

| | D | p | G | $X_{eq}$ | CHF | L | $T_{inlet}$ | $T_{sat}$ | $\alpha_{max}$ |
|---|---|---|---|---|---|---|---|---|---|
| | [m] | [MPa] | [kg/m$^2$/s] | [-] | [MW/m$^2$] | [m] | [°C] | [°C] | [-] |
| Case 24 | 0.004 | 15.7 | 2000 | 0 | 3.465 | 0.5 | 180.15 | 345.8 | 0.829 |
| Case 6 | 0.008 | 15.7 | 2000 | 0 | 2.45 | 1 | 236.98 | 345.8 | 0.842 |
| Case 23 | 0.012 | 15.7 | 2000 | 0 | 2 | 1 | 293.86 | 345.8 | 0.855 |
| Case 25 | 0.016 | 15.7 | 2000 | 0 | 1.7324 | 1 | 314.81 | 345.8 | 0.846 |

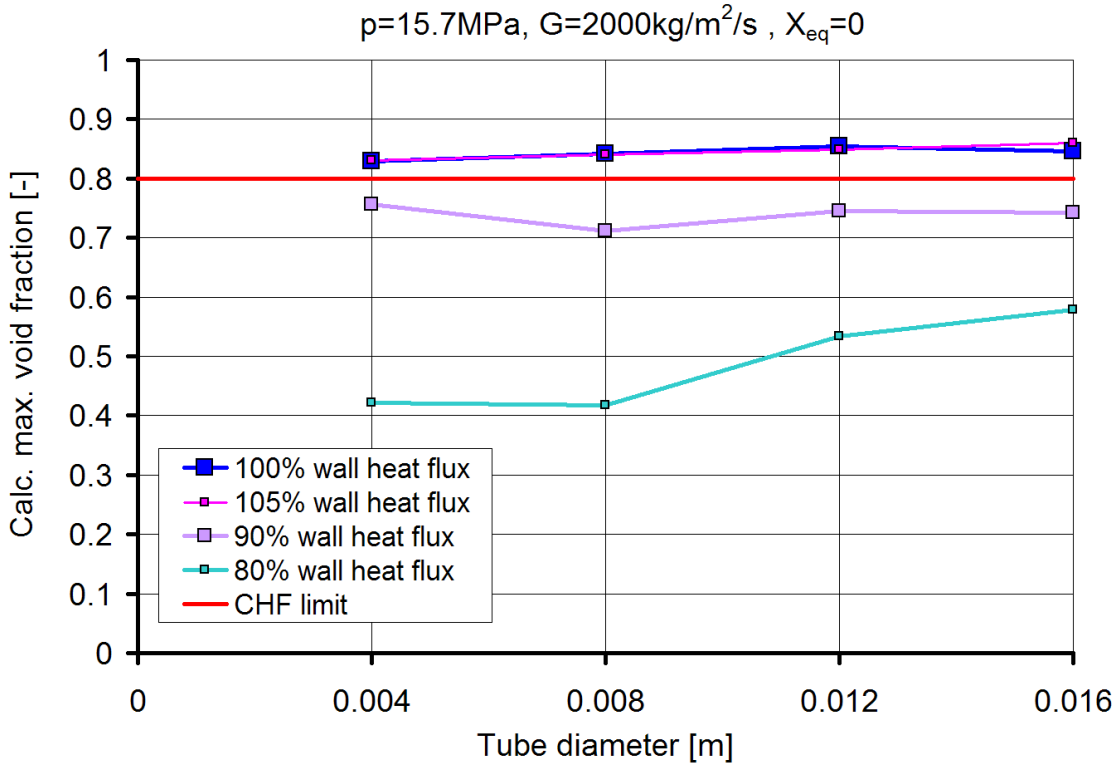


Fig. 10: Series 4 - Results

## 7. CONCLUSIONS

The NEPTUNE_CFD code with a generalized wall-heat-flux splitting model was used to simulate critical heat flux in tube geometry. The standard CHF tables produced by the Russian Academy of Sciences were used as the data set. A simple criterion based on a local void fraction equal to 0.8 was used to predict CHF. NEPTUNE could quite accurately predict CHF in cases with high mass fluxes and high pressures. The method did not work well for low mass fluxes (1000kg/m$^2$/s) and for low pressures (10MPa).

## REFERENCES


Collier: “Convective Boiling and Condensation”, McGraw-Hill (1981)

Groeneveld, D.C., Cheng, S.C., Doan, T.: “AECL-UO Critical Heat Flux Lookup Table”, *Heat Transfer Eng. 7*, 46-62, (1986)

Haynes, P.-A., Peturaud, P., Montout, M., Hervieu, E.: "Strategy for the Development of a DNB Local Predictive Approach Based on NEPTUNE CFD Software", *ICONE14*, Miami, Florida, July17-20, (2006)

Hewitt, G.F., Roberts, D.N.: "Studies of two-phase flow patterns by simultaneous flash and X-ray photography" AERE-M2159, (1969)

Hsu, Y.Y.: "On The Size Range of Active Nucleation Cavities on a Heating Surface", *J. Heat Transfer 84*, pp.207-216 (1962)

Ishii, M.: "Two-fluid model for two-phase flow", *Multiphase Science and Technology*, Eds. Hewitt, G.F., Delhaye, J.M., Zuber, N., Vol.5, pp 1-58, (1990)

Koncar, B., Borut, M.: "Wall-to-Fluid Transfer Mechanisms in Boiling Flows", *XCFD4NRS - Experiments and CFD Code Applications to Nuclear Reactor Safety*, OECD/NEA & IAEA Workshop, CEA Grenoble, France, 10 - 12 September (2008)

Kurul, N., Podowski, M.Z.: "Multidimensional Effects in Forced Convection Subcooled Boiling", *Proceedings of the 9th International Heat Transfer Conference*, Jerusalem, Israel, 21-26 August (1990)

Lance M., Lopez de Bertodano M.: "Phase distribution phenomena and wall effects in bubbly two-phase flows", *Multiphase Science and Technology* 8, pp. 69-123 (1994)

Lavieville, J., Quemerais, E., Mimouni, S., Boucker, M., Mechitoua, N.: "NEPTUNE CFD V1.0 Theory Manual", EDF (2005)

Le Corre J.-M., Yao, S.-C., Amon C. H.: "A mechanistic model of critical heat flux under subcooled flow boiling conditions for application to one- and three-dimensional computer codes" *Nuclear Engineering and Design* 240, pp. 235–244, (2010)

Morel C., Yao W., Bestion D.: "Three dimensional modelling of boiling flow for the NEPTUNE code", *NURETH-10*, Seoul, Korea, Oct.5-9 (2003)

Morel, C.: "Validation of NURESIM CFD against DEBORA Tests Close to CHF Conditions", *NURESIM Project SP2*: Deliverable D2.2.1.3. European Commission, 6th EURATOM Framework Programme 2005-2008, December (2006)

Podowski, M. Z., Podowski R. M.: "Mechanistic Multidimensional Modeling of Forced Convection Boiling Heat Transfer", *Science and Technology of Nuclear Installations*, Article ID 387020, Vol. (2009)

Shin, B.S., Chang, S.H.: "CFD analysis on subcooled boiling flow in 2x3 rod bundle with and w/o mixing vane under CHF conditions", *NUTHOS-7: The 7th International Topical Meeting on Nuclear Reactor Thermal Hydraulics, Operation and Safety* Seoul, Korea, October 5-9, (2008)

Taitel, Y., Bornea, D., Dukler, A.E.: "Modelling flow pattern transitions for steady upward gas-liquid flow in vertical tubes", *AIChE J.* 26:345 (1980)

Troshko A., Schowalter D., Guetari C.: "CFD Validation Benchmark of Subcooled Nucleate Boiling Under Near Saturation Conditions", *NURETH-12*, Pittsburgh, Pennsylvania, USA, Sept 30-Oct 4, (2007)

Ünal, H.C.: "Maximum bubble diameter, maximum bubble growth time and bubble growth rate during subcooled nucleate flow boiling of water up to 17.7MW/m$^2$", *Int. J. Heat Mass Transfer 19*, pp.643-649, (1976)

Vyskocil, L., Macek, J.: “Boiling Flow Simulation in NEPTUNE_CFD And FLUENT Codes”, *XCFD4NRS, Experiments and CFD Code Applications to Nuclear Reactor Safety,* OECD/NEA & IAEA, Grenoble, France, 10 - 12 September (2008)

Weisman J., Pei B.S.: “Prediction of Critical Heat Flux in Flow Boiling at Low Qualities”, *Int. J. Heat Mass Transfer 26,* pp. 1463-1477 (1983)

Working Party of the Heat and Mass Transfer Section of the Scientific Council of the USSR Academy of Sciences: “Tabular data for calculating burnout when boiling water in uniformly heated round tubes” *Teploenergetika*, 23 (9), 90-92, (1976)

Yao W., Morel C.: “Volumetric interfacial area prediction in upward bubbly two-phase flow”, *Int. J. Heat and Mass Transfer* 47, pp. 307-328 (2004)

Yao W., Morel C.: “Prediction of parameters distribution of upward boiling two-phase flow with two-fluid models”, *ICONE10-22463,* Arlington, VA, April 14-18 (2002)